IEEE Photonics Journal
An IEEE Photonics Society Publication

Open Access

Study on the Photoacoustic Technology to Simultaneous In-Situ Detection of the Cavity Ring-Down Spectrum for Multi-Optical Parameters

Volume 12, Number 2, April 2020

Hua-Wei Jin
Ren-Zhi Hu
Pin-Hua Xie
Chong-Chong Huang
Feng-Yang Wang
Chuan Lin

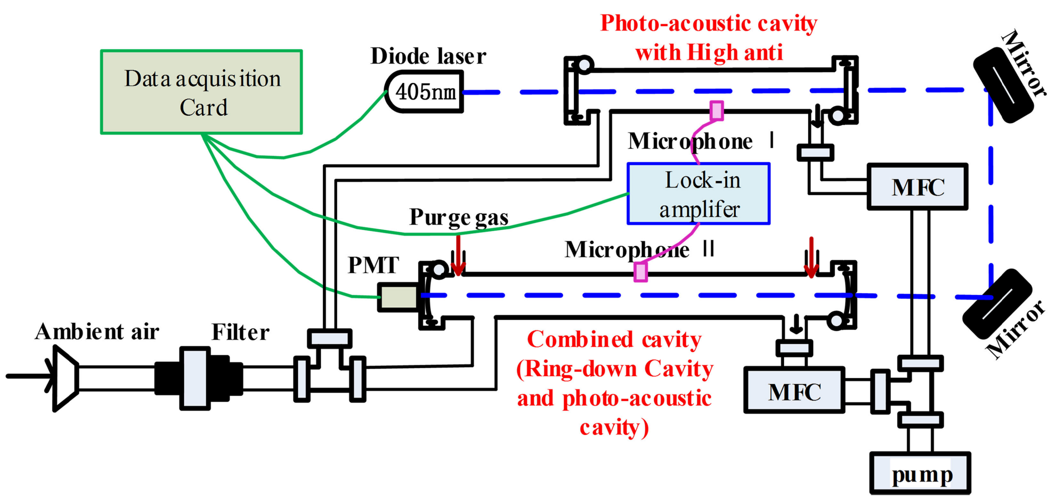

DOI: 10.1109/JPHOT.2020.2969226

IEEE photonics SOCIETY
IEEE

Study on the Photoacoustic Technology to Simultaneous In-Situ Detection of the Cavity Ring-Down Spectrum for Multi-Optical Parameters

Hua-Wei Jin,[1,2,6] **Ren-Zhi Hu**,[1,6] **Pin-Hua Xie**,[1,3,4,5]
Chong-Chong Huang,[1,6] **Feng-Yang Wang**,[1,6] **and Chuan Lin**[1]

[1]Key Laboratory of Environmental Optics & Technology, Anhui Institute of Optics and Fine Mechanics, Chinese Academy of Sciences, Hefei 230031, China
[2]Anhui Key Laboratory of Mine Intelligent Equipment and Technology, Anhui University of Science and Technology, Huainan 232001, China
[3]Institutes of Physical Science and Information Technology, Anhui University, Hefei 230601, China
[4]CAS Center for Excellence in Regional Atmospheric Environment, Institute of Urban Environment, Chinese Academy of Sciences, Xiamen, Fujian 361000, China
[5]University of Chinese Academy of Sciences, Beijing 100049, China
[6]University of Science and Technology of China, Hefei 230026, China

DOI:10.1109/JPHOT.2020.2969226

Manuscript received November 13, 2019; revised December 24, 2019; accepted January 21, 2020. Date of publication January 24, 2020; date of current version March 5, 2020. This work is supported by the National Natural Science Foundation of China under Grants 91644107, 61575206, 51904009, and 41905130, in part by the National Key R&D Program of China under Grants 2017YFC0209401, 2017YFC0209403, and 2017YFC0209902, in part by the Outstanding Young Talents Program of Anhui University of China under Grants gxyq2019022, and in part by the Natural Science Foundation Program of Anhui Province of China under Grant 1908085QD159. Corresponding authors: Ren-Zhi Hu; Pin-Hua Xie (e-mail: rzhu@aiofm.ac.cn; phxie@aiofm.ac.cn).

Abstract: A simultaneous in-situ detection technique to obtain multi-optical parameters was proposed. The same 403.56 nm, low power, blue diode laser was used to conduct the cavity ring-down spectroscopy and photoacoustic spectroscopy, which were coupled. Four photoacoustic spectra were applied to the simultaneous in-situ detection of the cavity ring-down spectrum, which were systematically compared and analyzed for the first time. And the main performance of the systems varied with the arrangement of the photoacoustic pool. The results reveal that the photoacoustic response was optimized by the high reflectivity mirror with the pool constant of 1450.64 (Pα·cm)/W and the signal sensitivity of 0.2562 μv/ppb. The intensity value of the photoacoustic pool inside the cavity ring down was superimposed to 48.45% of the initial intensity. The corresponding experimental results were consistent with the theoretical analysis and shown the coupled cavity could suitable for simultaneous in-situ measurement of high concentration. The coupled two detection techniques detected different optical parameters and thus provided a new method for the simultaneous in-situ detection of the multi-optical parameters of specific atmospheric components.

Index Terms: Photoacoustic technology, cavity ring-down spectroscopy, blue diode laser, coupled spectrum, simultaneous in-situ detection.

1. Introduction

With the development of society and the economy, environmental pollution has seriously threatened people's physical and mental health. Thus, it is extremely urgent that we determine the pollution mechanism in real time [1], especially the impact of the optical parameters of specific components of the atmosphere on atmospheric oxidation [2], regional transmission [3], [4], disease prevention and control [5], and pollution sources [6]. Taking atmospheric aerosols as an example, optical parameters such as extinction, scattering, and absorption coefficients are of vital importance to the study of the prevention and controlling mechanism of atmospheric pollution [7]. Thus, laser radar technology [8], filter technology [9], refractive index technology [10], integral sphere technology [11], tunable semiconductor laser absorption spectroscopy [12], differential absorption spectroscopy [13], [14], cavity enhanced absorption spectroscopy [15], [16], cavity ring-down spectroscopy (CRDS) [17], [18], and photoacoustic spectroscopy (PAS) [19]–[21] as well as other optical detection methods have emerged. However, a single instrument for the measurement of a single parameter does not guarantee the same measurement standard, and the existing multi-parameter synchronous detection equipment is more confined to the simultaneous superposition measurement of different parameters at the same time, such as the detection of the extinction coefficient and the scattering coefficient of the double integral and ball pool, the integrating sphere and cavity enhanced, the integrating sphere and cavity ring-down technology, etc. [11], [22], [23]. In addition, these indirect measurement methods, which are based on extinction and scattering, are affected by many factors, so they cannot reflect the influence of sampling loss, cavity differences, detection sources (excitation light source), and other factors. In the field of atmospheric detection, research into multi-optical parameter integrated synchronous conventional observation technology is still rare and imperfect. In addition, there is no scientific instrument for the direct simultaneous in-situ measurement of multi-optical parameters.

Photoacoustic spectroscopy and cavity ring-down spectroscopy are important trace gas detection techniques, which are widely applied in the field of atmospheric science [23]. In this manuscript, we develop a cavity detection technique with synchronous in situ detection. The same 403.56 nm, low power, blue diode laser was used to conduct the ring-down spectroscopy and the photoacoustic spectroscopy which be coupled. Four photoacoustic spectra were used in the simultaneous in-situ detection of the cavity ring-down spectrum and were studied using comparative analysis for the first time. In addition, the pool constant, signal sensitivity, and photoacoustic response were systematically compared and analyzed. A method for obtaining the extinction and absorption coefficients of specific components of the atmosphere with synchronous in-situ detection is proposed.

2. Measuring Principles

2.1 Principle of Coupled Spectroscopy Measurement

Based on the photoacoustic effect, photoacoustic spectroscopy technology aims to form a heat source to inspire the sound source of the perturbed gas through the absorption of a certain power P_0 of light. The absorption coefficient α_{abs} of a specific gas can be obtained through the detection of the sound source [24], [25]. If the photoacoustic signal S_{PA} is detected by microphone (sensitivity S_m). The absorption coefficient α_{abs} of a specific measured gas, which is based on the photoacoustic spectrum, can be expressed as

$$\alpha_{abs} = \frac{S_{PA}}{C_{cell} P_0 S_m} \tag{1}$$

Cavity ring-down spectroscopy is mainly based on the Lambert Beer's Law. The attenuation signal of the optical intensity of the optical resonator (with a high mirror at both ends) is fitted exponentially. The relationship between the ring-down time of the light intensity and the measured object can be established based on the length d of the optical resonator, the operating length L_s of the measured object, the ring-down time τ, etc. The extinction coefficient α_{ext} of the specific

$$S_n = \frac{I_0(1-R)(1-R^n)}{1-R} = I_0(1-R^n)$$

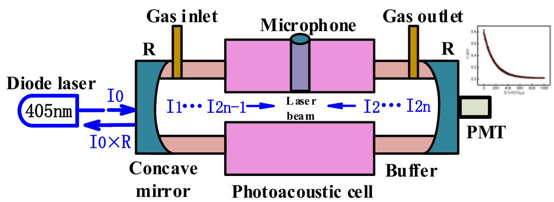

Fig. 1. Superposition analysis of the light intensity based on a high reflection mirror.

measured gas, which is based on the cavity ring-down spectrum, can be expressed as [26]

$$\alpha_{ext} = \frac{d}{cL_s}\left(\frac{1}{\tau(\upsilon) - \tau_0}\right) \tag{2}$$

The main structure of the coupled system is based on the cavity ring-down system, which adopts the same light source, light path, gas path and main cavity. The main difference lies in the modification of the intermediate cavity into the resonant cavity required by the photoacoustic cavity. Microphones and other detectors are arranged in the cavity to realize photoacoustic detection. Thus, based on equations (1) and (2), the scattering coefficient α_{scat} of the specific measured gas, which is based on the coupled system, can be expressed as

$$\alpha_{scat} = \alpha_{ext} - \alpha_{abs} \tag{3}$$

2.2 Superposition Analysis of the Light Intensity Based on the High Reflection Mirror

The two ends of the traditional photoacoustic cavity are mostly sealed with a quartz window [27]–[29]. If a concave mirror with a higher reflectivity R (a high reflectivity mirror) is used to replace the quartz window, the light intensity characteristics of the areas internal and external to the cavity will be altered, as shown in Fig. 1. The light emitted by the specific laser is reflected $I_0 \times R$ before entering the cavity, and the remaining transmitted light $I_1 = I_0(1 - R)$ is reflected back and forth n times in the cavity. Thus, the superimposed laser light intensity S_n is

$$S_n = \frac{I_0\,(1-R)\,(1-R^n)}{1-R} = I_0\left(1-R^n\right) \tag{4}$$

Where I_0 is the initial light intensity of the inlet cavity, R is the reflectivity of the high reflectivity mirror, and n is the number of laser reflections between the high reflectivity mirrors. S_n is proportional to n for a certain R. Therefore, in order to obtain the relationship between the light intensity and something, it is necessary to calibrate and test the reflectivity R of the high reflector and the reflection number n of the laser between the high reflectivity mirrors. NO_2 gas with a known concentration (0.204 ppm) was used as the standard gas. The length of the cavity in this system was 780 mm, and the length of the sample was 695 mm. The corresponding coefficient α was calculated to be $2.982 \times 10^{-6}\ cm^{-1}$, and the ring down time τ was determined to be 4.2 μs from a laboratory test. Thus, the reflectivity of the high reflectivity mirror ($R = 1 + \alpha L_s - \frac{d}{c\tau}$) was 99.959%, and the number of reflections ($n = \frac{\tau c}{d}$) was 1616. Based on the formula (4), the superimposed laser intensity S_n is 48.45% of the initial intensity.

If the photoacoustic pool is arranged inside and outside the ring down cavity, it will have different response characteristics. 1) For external-cavity detection, the two ends of the photoacoustic pool are still sealed with quartz window plates. The cavity arranged between the laser and the high mirror will receive both the laser light intensity and the high mirror reflected light intensity $I_0 \times R$. The light intensity value is nearly doubled, and the photoacoustic response characteristics are

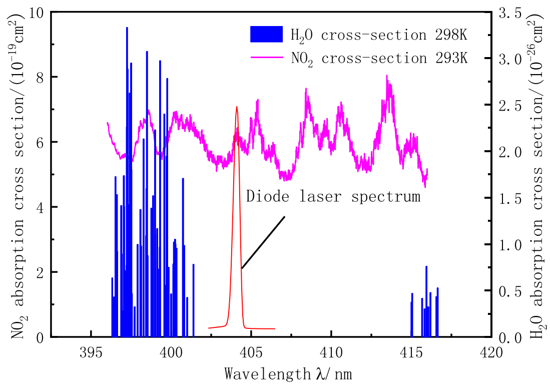

Fig. 2. Cross sections of the NO_2, H_2O and the diode laser spectrum.

improved. This type of photoacoustic pool is called a high reflective acoustic cavity. 2) For intra-cavity detection, the unsealed photoacoustic pools at both ends are connected in series between the high reflectivity mirror and are sealed by a high reflectivity mirror. The synchronous detection of the photoacoustic signal and the ring-down signal in the same cavity is performed. This type of photoacoustic pool is called a coupled photoacoustic cavity.

2.3 Laser Selection

The absorption cross section σ is very important to obtaining the correlation coefficient. For different gases, the absorption cross section varies with wavelength and is accompanied by a disturbance gas. Therefore, it is necessary to comprehensively consider the selection of the laser. In order to facilitate the study of the coupling detection technology with the cavity ring-down and photoacoustic spectra, NO_2 was introduced as a test gas. The absorption cross section of NO_2 is between 390 nm and 420 nm (Bogumil, 2003, 293 K) [30], as shown in Fig. 2. The absorption cross section of NO_2 near 403 nm has a strong absorption peak, and the influence of water vapor and interfering gases is relatively small. Therefore, a blue diode laser with a central wavelength of 403.56 nm and a power of 120 nW was selected as the light source.

3. Experimental Setup

In order to compare and analyze the response characteristics of the coupled photoacoustic cavity and the high-reflective photoacoustic cavity, a cavity ring-down and photoacoustic spectra synchronization test experimental system was constructed, as shown in Fig. 3. The system consists of a 403 nm diode laser (Shanghai xi long, China, DL-405), a photoacoustic cavity (independently designed, cylindrical cavity, L_c of 120 mm, R_c of 8 mm, a ring-down cavity (independently designed, 780 mm long), a reflector (Thorlabs),a detector, a signal processing module and a gas-path module. The blue laser produces a laser beam with a specific frequency and duty cycle using square wave modulation.

The laser passed through the highly reflective acoustic cavity, the plane reflector and the cavity successively. The system mainly depended on adjusting the ring down time of the ring down cavity system and observing the laser spots on the mirror to ensure the consistency of the light path of the series mode. The measured gas was absorbed and excited and produced the photoacoustic signal of the high reflection cavity, the photoacoustic signal of the coupled cavity, and the optical intensity signal of the ring-down cavity. The photoacoustic signals of the highly reflective cavity and the coupled cavity were detected using 2 microphones (I and II) (Beijing prestige, China, MP201), the signals of which were collected by the double-channel phase-locked amplifier (Sine Scientific Instrument, China, OE1022D). The optical intensity signal of the ring-down cavity was

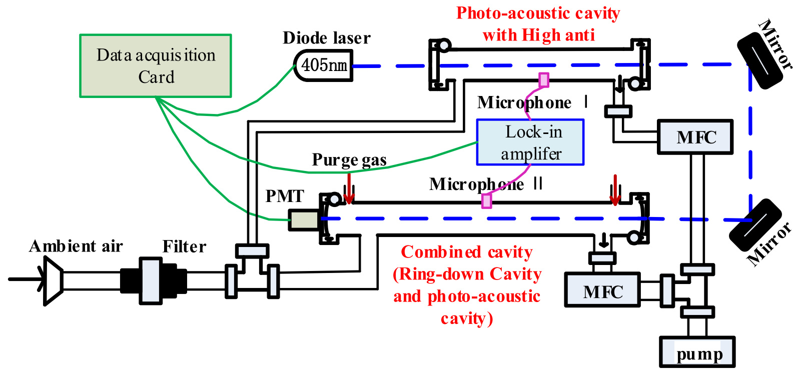

Fig. 3. System of the ring-down cavity and photoacoustic spectrum synchronization measurement.

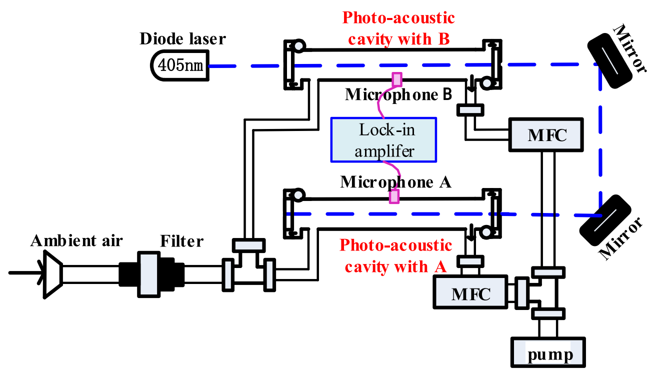

Fig. 4. Diagram of the experimental system for the dual photoacoustic spectrum synchronization measurement.

detected using a photomultiplier tube (H10721-210, Japan, Hamamatsu Photonics), the signals of which was collected by the LabVIEW software. The gas-path system used a vacuum pump (NMP860KNE, KNF) at the back of the gas-path to extract the air. The measured gas entered the two cavities through a three-way pipe, and the flow rate was controlled by the mass flow-meter (Seven star Huachuang, China, CS200).

In addition, in order to more effectively carry out the comparative study of the response characteristics of different photoacoustic cavities, a dual photoacoustic spectral system without a high reflectivity mirror based on the same type of light source was built, as shown in Fig. 4. The blue-diode laser passed through the traditional photoacoustic systems B and A. The difference in this system was the collimation control, the quartz window plate control and the cavity's fineness. The alignment of photoacoustic system A can be adjusted by two planar mirrors.

4. Results and Discussion

4.1 Performance Analysis of the Coupled Ring-Down Cavity

The length of the ring-down cavity was 780 mm, the length of the sample was 695 mm, and their ratio R_L was 1.122. The ring-down time τ with 2.5 M sampling frequency was 11.43639 μs $\pm$ 0.034199 μs, i.e., $\tau_0 = 11.43639\ \mu$s and $\sigma(\tau_0) = 0.034199\ \mu$s. Thus, the minimum detection limit was

$$[A]_{\min} = \frac{R_L}{c\sigma}\frac{(\tau_0 - \tau)_{\min}}{\tau_0^2} \approx \frac{R_L}{c\sigma}\frac{\sqrt{2}\sigma(\tau_0)}{\tau_0^2} = 0.9335\,\text{ppb} \tag{5}$$

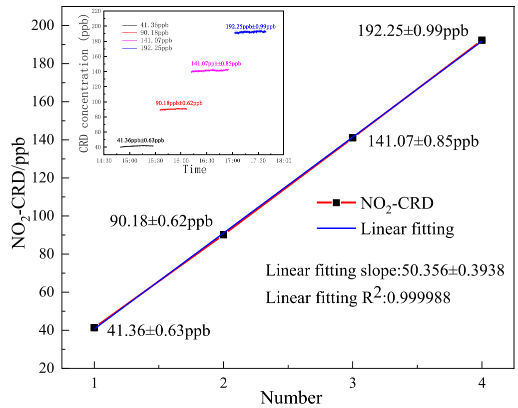

Fig. 5. Performance analysis of the coupled ring-down cavity.

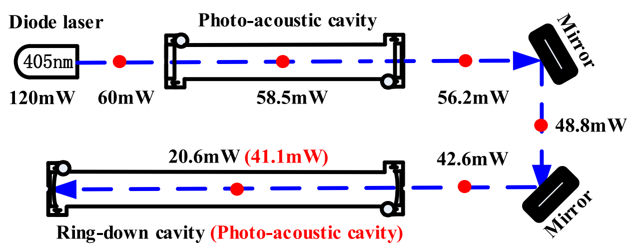

Fig. 6. Power distribution test.

The concentration gradient of the ring-down cavity was tested and is shown in Fig. 5. The standard NO_2 gas was injected into the cavity with volume fractions of 41.36 ppb, 90.18 ppb, 141.07 ppb and 192.25 ppb. The corresponding concentration fluctuations were 0.63 ppb, 0.62 ppb, 0.85 ppb and 0.99 ppb, respectively. The linear gradient was good, and the R^2 was close to 1.

4.2 Performance Analysis of the Traditional Photoacoustic Cavity

One of the characteristics of photoacoustic spectroscopy is that the response is proportional to the excitation laser's power. Therefore, based on the optical path loss, the power distribution of the blue diode laser at different positions on the optical path is shown in Fig. 6. The output power of the blue diode laser was 120 mW. The output power was modulated to 60 mW after the square wave modulation with a duty cycle of 50%. The power of the laser was reduced to 58.5 mW after passing through the first quartz glass window of the first photoacoustic cavity. Then, the laser passed through the second surface of the first photoacoustic cavity, the first surface planar mirror, and the second surface planar mirror. The corresponding powers were 56.2 mW, 48.8 mW and 42.6 mW, respectively. Finally, if the cavity was a photoacoustic cavity, the power after passing through the quartz glass was 41.1 mW. While if it was a cavity ring-down, the cumulative power $P_{v-v\_coupling}$ in the coupling cavity was 20.6 mW.

The photoacoustic response varies with the modulation frequency of the laser, and is maximized at the resonant frequency of the cavity. Theoretically, the resonant frequency is determined by $v/2L_0$. Considering the influencing environmental factors, the end response, and the process, there are certain differences in the resonant frequencies of the different arrangements. The resonance frequency of the laser was calibrated using a square wave with a specific amplitude. Through fitting, the resonance frequency of the high anti-cavity was 1.29 kHz, as shown in Fig. 7(a). Similarly, the resonant frequencies of cavity A and cavity B were 1.39 kHz and 1.35 kHz respectively.

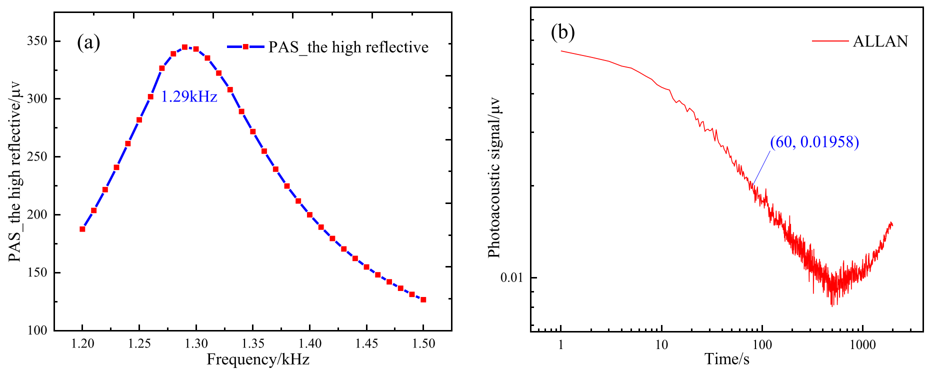

Fig. 7. (a) Frequency response of the photoacoustic cavity; (b) Detection limit analysis of the photoacoustic cavity.

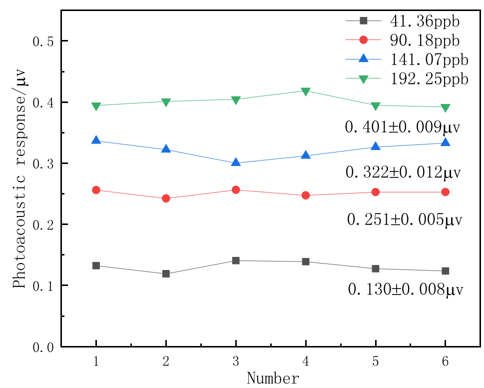

Fig. 8. Repeated test results of the coupling cavity.

ALLAN variance analysis was conducted to detect the limit analysis of the traditional photoacoustic cavity, as shown in Fig. 7(b).

The lower limit of the measurement was 0.01968 μv (60 s) as can be seen from the figure. According to the system calibration gradient slope [22], the corresponding volume fraction is 1.22 ppb. The detection limit of the independently arranged optical sound cavity was 3.67 ppb (3σ principle), which meets the measurement requirements of the ambient atmosphere.

4.3 Comparative Analysis of the Different Photoacoustic Cavities

The gas concentrations are increased from low to high, and the responses of the photoacoustic systems are repeated for 6 times, and the average values are taken. For example, the data of coupled cavity can be seen in Fig. 8, and the other cavities are similar. The figure shows the repeatability of coupled cavity is very good and the measurement scheme proposed in this paper is reliable.

Since the scattering coefficient of NO_2 due to the laser is extremely small, the measured coefficients of the ring-down cavity spectrum and the photoacoustic spectrum should theoretically be consistent. For the coupled photoacoustic cavity, the background was 0.91 μv, and the sensitivity of the microphone $S_{m\_coupled}$ was 52.5 mv/P_{α}. When the NO_2 with a volume fraction of 0.14107 ppm was passed into the coupled cavity, the photoacoustic response $S_{PA\_coupled\,\Delta}$ was 0.32 μv.

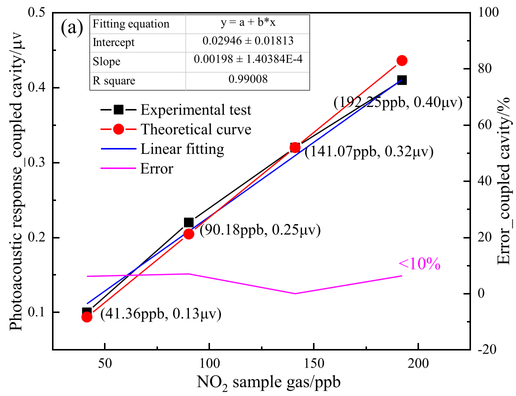

(a) Photoacoustic coupled cavity.

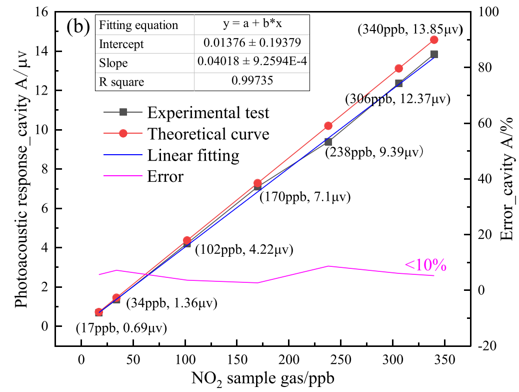

(b) Photoacoustic cavity A.

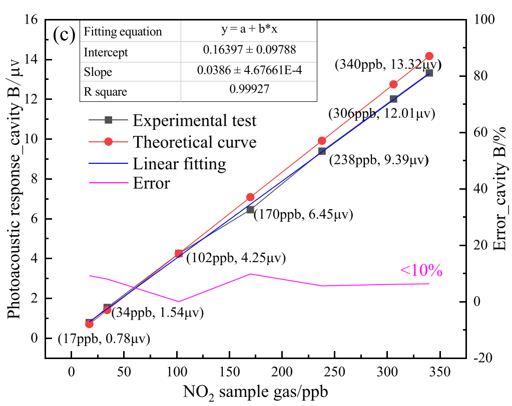

(c) Photoacoustic cavity B.

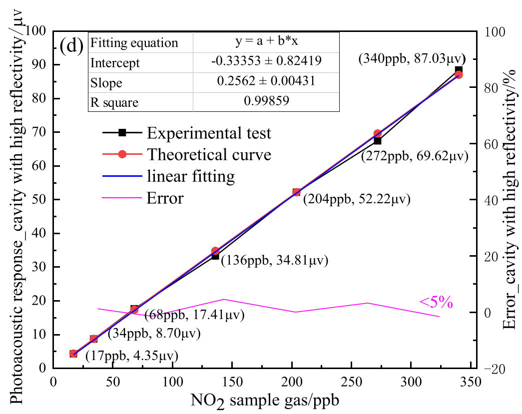

(d) High reflectivity photoacoustic cavity.

Fig. 9. Performance analysis of the photoacoustic cavity.

The following relationships were determined:

$$\rho_{(mg/m^3)} = \frac{\alpha_{volume} \times M_{NO_2}}{24.5} = 0.26487\ mg/m^3 \tag{6}$$

$$A_{concentration} = \left(\frac{\alpha_{volume}}{24.5}\right) \times 10^{-3} \times N_A = 3.47 \times 10^{12}\ mole/cm^3 \tag{7}$$

$$\alpha = \sigma \times A = 2.062 \times 10^{-6}\ cm^{-1} \tag{8}$$

$$C_{cell\_coupled} = \frac{S_{PA_{coupled}\Delta}}{S_{m\_coupled}\alpha P_{v-v\_coupled}} = 143.5P_\alpha \cdot cm/W \tag{9}$$

$$\alpha_{volume\_coupled} = 4.4 \times 10^6 S_{PA_{coupled}\Delta} \tag{10}$$

In order to evaluate the performance of the system in terms of accuracy and linearity, four different concentration levels of NO_2 gas mixtures (41.36 ppb, 90.18 ppb, 141.07 ppb and 192.25 ppb) were fed into the system. The resultant signal amplitudes from the system were 0.13 μv, 0.25 μv, 0.32 μv, and 0.40 μv, respectively, as shown in Fig. 9(a). Some conclusions about linear fitting were reached. (1) The linearity of the experimental test data is very good, and R^2 reaches to 0.99008. (2) The fitting slope is 0.00198, which is consistent with the theoretical model slope of 0.002268, and the slope error is less than 15%. (3) The results are consistent with the theory, and the error in

TABLE 1
Comparative Analysis of Photoacoustic Cavities With Different Arrangements

Parameter	Photoacoustic cavity A	Photoacoustic cavity B	Photoacoustic cavity with high reflectivity	Photoacoustic coupled cavity
$S_m\ (mv/P_\alpha)$	58.5	52.5	53.7	52.5
$\alpha(\times 10^{-6} cm^{-1})$	1.4909	1.4909	2.982	2.06193
$P_{v-v}(mW)$	41.1	58.5	112.4	41.1
$S_{PA}(\mu v)$	4.22	4.25	26.11	0.32
$C_{cell}(P_\alpha \cdot cm/W)$	**1177.243**	928.18	**1450.64**	71.9242
Fitting R^2	0.9974	0.9993	0.9986	0.9901
Fitted slope	0.0402	0.0386	0.2562	0.002
Theoretical slope	0.0414	0.0417	0.2560	0.0023
Slope error	< 6%	< 8%	< 1%	< 15%
Data error	< 5%	< 10%	< 5%	< 10%

the model data is less than 10%. Because of the influencing factors, e.g., the laser loss, the cavity fineness difference, the mirror interference, different photoacoustic responses were obtained for the photoacoustic cavities with different layouts. The different photoacoustic responses are shown in Fig. 9(b)–(d).

4.4 Discussion

In order to evaluate the performance of the photoacoustic cavities with different arrangements, the test analysis results shown in Table 1 were compared. Compared to photoacoustic cavity A, which has a pool constant of 1177.243 $P_\alpha \cdot cm/W$, the pool constant of photoacoustic coupled cavity in the same position was 69.39164 $P_\alpha \cdot cm/W$. Theoretically, the photoacoustic signal in the coupled cavity can only reach 5.894% of the response of photoacoustic cavity A. However, the actual test revealed that when the absorption coefficients of NO_2 were $1.4909 \times 10^{-6}\ cm^{-1}$ and $2.06193 \times 10^{-6}\ cm^{-1}$, the corresponding photoacoustic values were 4.22 μv and 0.32 μv, respectively. The photoacoustic signal in the coupled cavity was 5.483% of the photoacoustic signal in photoacoustic cavity A. The actual test was consistent with the theoretical analysis, and the error was less than 7%, which verifies the theoretical analysis results of the coupled cavity.

Several further conclusions were reached: (1) The pool constants of the photoacoustic cavities are different, with the constants of the coupled cavity, cavity B, cavity A, and the cavity with high reflectivity in descending order. The pool constant is optimized to 1450.64 $P_\alpha \cdot cm/W$ by the high reflectivity mirror. (2) The linearity of the four photoacoustic cavities with different arrangements is very good, i.e., R^2 is greater than 0.99. (3) The fitted slope of the photoacoustic cavity with high reflectivity is the largest. This indicates that the signal sensitivity is maximized to 0.2562 μv/ppb by the high reflectivity mirror. (4) The fitted slope is close to the slope of the theoretical analysis. However, the errors in the slope and data are small and different. (5) The coupled cavity has the advantage of the application of simultaneous in-situ detection. While the photoacoustic coupled cavity is suitable for measurement of high concentrations. This will be of great application value for the coal mine dust detection and other occasions. (6) Compared with the detection of individual cavity, the coupling cavity system can ensure the consistency of the interference factors in the measurement of different parameters, so as to improve the reference value of different parameters.

(7) When multiple optical parameters need to be detected, taking aerosol detection as an example, the coupling cavity system will improve the correlation between the extinction coefficient and the absorption coefficient detection of aerosol, so as to obtain the single scattering albedo, aerosol refractive index, visibility and other optical properties. However, it can be predicted that if the measured gas is gas or low-concentration aerosol, the advantage is smaller because the extinction coefficient and absorption coefficient are close to each other. (8) Compared with photoacoustic cavity A and cavity B, the photoacoustic cavity with high reflectivity has a superior slope error, data error and pool constant. However, it should be noted that the photoacoustic cavity needs a high reflection mirror for power superposition, which has a higher cost.

5. Conclusion

In this manuscript, we developed a cavity detection technique with simultaneous in situ detection. The same 403.56 nm, low power, blue diode laser was used to conduct the cavity ring-down spectroscopy and photoacoustic spectroscopy, which were coupled to detect multi-optical parameters. Four photoacoustic spectra were applied to the simultaneous in-situ detection of the cavity ring-down spectrum, which were systematically compared and analyzed for the first time. And the main performance of the systems varied with the arrangement of the photoacoustic pool. The results reveal that the photoacoustic response was optimized by the high reflectivity mirror. The corresponding experimental results were consistent with the theoretical analysis and shown the coupled cavity could suitable for simultaneous in-situ measurement of high concentration. The coupled two detection techniques detected different optical parameters and thus provided a new method for the simultaneous in-situ detection of the multi-optical parameters of specific atmospheric components.

References

[1] R. Y. Yang and W. D. Chen, "Spatial correlation, influencing factors and environmental supervision mechanism construction of atmospheric pollution: an empirical study on SO_2 emissions in china," *Sustainability*, vol. 11, pp. 1742/1–1742/13, 2019.

[2] Z. Peng, J. Lee-Taylor, J. J. Orlando, G. S. Tyndall, and J. L. Jimenez, "Organic peroxy radical chemistry in oxidation flow reactors and environmental chambers and their atmospheric relevance," *Atmos. Chemistry Phys.*, vol. 19, pp. 813–834, 2019.

[3] Q. Q. Hong *et al.*, "Evolution of the vertical structure of air pollutants during winter heavy pollution episodes: The role of regional transport and potential sources," *Atmos. Res.*, vol. 228, pp. 206–222, 2019.

[4] E. Potier *et al.*, "Characterizing the regional contribution to PM10 pollution over northern France using two complementary approaches: Chemistry transport and trajectory-based receptor models," *Atmos. Res.*, vol. 223, pp. 1–14, 2019.

[5] H. Paramesh, "Air pollution and allergic airway diseases: Social determinants and sustainability in the control and prevention," *Indian J. Pediatrics*, vol. 85, pp. 284–294, 2018.

[6] P. Wang, Y. A. Hu, and H. F. Cheng, "Municipal solid waste (MSW) incineration fly ash as an important source of heavy metal pollution in China," *Environ. Pollut.*, vol. 252, pp. 461–475, 2019.

[7] L. Ferrero *et al.*, "Aerosol optical properties in the Arctic: The role of aerosol chemistry and dust composition in a closure experiment between lidar and tethered balloon vertical profiles," *Sci. Total Environ.*, vol. 686, pp. 452–467, 2019.

[8] R. Volkamer *et al.*, "Aircraft measurements of BrO, IO, glyoxal, NO_2, H_2O, O-2-O-2 and aerosol extinction profiles in the tropics: comparison with aircraft-ship-based in situ and lidar measurements," *Atmos. Meas. Techn.*, vol. 8, pp. 2121–2148, 2015.

[9] A. Pandey, S. Pervez, and R. K. Chakrabarty, "Filter-based measurements of UV-vis mass absorption cross sections of organic carbon aerosol from residential biomass combustion: Preliminary findings and sources of uncertainty," *J. Quantitative Spectroscopy Radiative Transfer*, vol. 182, pp. 296–304, 2019.

[10] K. Alam, T. Trautmann, T. Blaschke, and F. Subhan, "Changes in aerosol optical properties due to dust storms in the middle east and southwest asia," *Remote Sens. Environ.*, vol. 143, pp. 216–227, 2014.

[11] S. Singh, M. N. Fiddler, D. Smith, and S. Bililign, "Error analysis and uncertainty in the determination of aerosol optical properties using cavity ring-down spectroscopy, integrating nephelometry, and the extinction-minus-scattering method," *Aerosol Sci. Technol.*, vol. 48, pp. 1345–1359, 2019.

[12] L. Dong *et al.*, "Compact TDLAS based sensor design using interband cascade lasers for mid-IR trace gas sensing," *Opt. Express*, vol. 24, pp. A528–A535, 2016.

[13] W. R. Espinosa *et al.*, "Retrievals of aerosol size distribution, spherical fraction, and complex refractive index from airborne in situ angular light scattering and absorption measurements," *J. Geophysi. Res.-Atmos.*, vol. 124, pp. 7997–8024, 2019.

[14] H. Irie *et al.*, "Evaluation of MAX-DOAS aerosol retrievals by coincident observations using CRDS, Lidar, and sky radiometer in Tsukuba, Japan," *Atmos. Meas. Techn.*, vol. 8, pp. 2775–2788, 2019.

[15] J. Duan *et al.*, "Development of an incoherent broadband cavity-enhanced absorption spectrometer for in situ measurements of HONO and NO_2," *Atmos. Meas. Techn.*, vol. 11, pp. 4531–4543, 2018.

[16] X. Z. H. Xu *et al.*, "Three-wavelength cavity-enhanced albedometer for measuring wavelength-dependent optical properties and single-scattering albedo of aerosols," *Opt. Express*, vol. 26, pp. 33484–33500, 2019.

[17] H. Fuchs, W. P. Dube, B. M. Lerner, N. L. Wagner, E. J. Williams, and S. S. Brown, "A sensitive and versatile detector for atmospheric NO_2 and NO_x based on blue diode laser cavity ring-down spectroscopy," *Environ. Sci. Technol.*, vol. 43, pp. 7831–7836, 2009.

[18] R. A. Washenfelder, N. L. Wagner, W. P. Dube, and S. S. Brown, "Measurement of atmospheric ozone by cavity ring-down spectroscopy," *Environ. Sci. Technol.*, vol. 45, pp. 2938–2944, 2011.

[19] J. Wojtas, A. Gluszek, A. Hudzikowski, and F. K. Tittel, "MidInfrared trace gas sensor technology cased on intracavity quartz-enhanced photoacoustic spectroscopy," *Sensors*, vol. 17, pp. 513/1–513/9, 2017.

[20] P. Patimisco *et al.*, "High finesse optical cavity coupled with a quartz-enhanced photoacoustic spectroscopic sensor," *Analyst*, vol. 140, pp. 736–743, 2015.

[21] X. K. Yin *et al.*, "Sub-ppb nitrogen dioxide detection with a large linear dynamic range by use of a differential photoacoustic cell and a 3.5 W blue multimode diode laser," *Sensors Actuators B-Chem.*, vol. 247, pp. 329–335, 2017.

[22] A. Uchiyama, "Method to retrieve single scattering properties of aerosols using multi-wavelength scattering and absorption coefficient data measured by integrating nephelometer and absorption photometer," *J. Meteorol. Soc. Jpn.*, vol. 92A, pp. 71–91, 2014.

[23] H. W. Jin *et al.*, "Study on photo-acoustic spectrum detection technology of respiratory dust absorption coefficient (Chinese)," *Spectroscopy Spectral Anal.*, vol. 39, pp. 1993–1998, 2019.

[24] J. Y. Sim, C. G. Ahn, C. Huh, K. H. Chung, E. J. Jeong, and B. K. Kim, "Synergetic resonance matching of a microphone and a photoacoustic cell," *Sensors*, vol. 17, pp. 804/1–804/10, 2017.

[25] A. Miklos, P. Hess, and Z. Bozoki, "Application of acoustic resonators in photoacoustic trace gas analysis and metrology," *Rev. Sci. Instrum.*, vol. 72, pp. 1937–1955, 2011.

[26] Z. Y. Li *et al.*, "Simultaneous measurement of NO and NO_2 by dual-channel cavity ring down spectroscopy technique," *Atmos. Meas. Techn.*, vol. 12, pp. 3223–3236, 2019.

[27] V. Zeninari, V. A. Kapitanov, D. Courtois, and Y. N. Ponomarev, "Design and characteristics of a differential Helmholtz resonant photoacoustic cell for infrared gas detection," *Infrared Phys. Technol.*, vol. 40, pp. 1–23, 1999.

[28] H. Zheng *et al.*, "Compact photoacoustic module for methane detection incorporating interband cascade light emitting device," *Opt. Exp.*, vol. 25, pp. 16761–16770, 2017.

[29] S. Voigt, J. Orphal, and J. P. Burrows, "The temperature and pressure dependence of the absorption cross-sections of NO_2 in the 250–800 nm region measured by Fourier-transform spectroscopy," *J. Photochemistry Photobiol. A-Chemistry*, vol. 149, pp. 1–7, 2002.

[30] D. C. M. Siciliani *et al.*, "Widely-tunable mid-infrared fiber-coupled quartz-enhanced photoacoustic sensor for environmental monitoring," *Opt. Express*, vol. 22, pp. 28222–28231, 2014.